Hittite Journal of Science and Engineering, 2018, 5 (Special Issue: Selected Papers from ULIBTK'17) 15-24
ISSN NUMBER: 2148-4171
DOI: 10.17350/HJSE19030000115

Design Manufacture and Performance Test of A Reciprocating Refrigeration Compressor

Yusuf Ali Kara[1] Deniz Uzunsoy[2] Hüseyin Lekesiz[1] Mustafa Gürkan Aydeniz[3]
[1] Bursa Technical University, Department of Mechanical Engineering, Bursa, TURKEY
[2] Bursa Technical University, Department of Metallurgical and Materials Science, Bursa, TURKEY
[3] Yıldız Technical University, Department of Electrical Engineering, İstanbul, TURKEY

ABSTRACT

The first generation of refrigeration compressors is reciprocating type compressors, the second generation is scroll type, and the third generation is screw type compressors that are available on the market. Although the need of semi-hermetic refrigeration compressor in Turkey market is 15000 per year, there is no any domestic manufacturer of semi-hermetic refrigeration compressor, and consequently Turkey imports all of the refrigeration compressors from abroad market. In this study, the performance and the manufacturing processes of the semi-hermetic refrigeration compressor that is designed and manufactured with a hundred percent of domestic opportunities are investigated. The performance tests of the compressor are done, the catalogue of the compressor is prepared and it is 12 % more efficient in comparison with equivalent European one.

Article History:
Received: 2018/01/23
Accepted: 2018/02/27
Online: 2018/09/07

***Correspondence to**: Yusuf Ali Kara*
Bursa Technical University, Department of Mechanical Engineering, Cevre Yolu Avenue, Bursa, Turkey
Tel: 0(224) 300 34 12
E-Mail:yusufali.kara@btu.edu.tr

Keywords:
Semi-hermetic reciprocating refrigeration compressor; Calorimetric performance setup for refrigeration compressor

INTRODUCTION

The heart of the vapor-compression refrigeration machines are the compressors. The widely used refrigeration compressor types are the reciprocating, screw, centrifugal and vane. Reciprocating compressors consist of suction and discharge valves regulating pumping process and pistons moving back and forth in cylinders. The screw, centrifugal and vane compressors all use rotating elements. The workhorse of refrigeration industry is the reciprocating compressor, built in sizes ranging from fractional-kilowatt to hundreds of kilowatts of refrigeration capacity. Reciprocating compressors may be single-cylinder or multi-cylinder. In multi-cylinder compressors the cylinders can be arranged V-type, W-type, or in-line type. The working principle of reciprocating compressors as follows; low-pressure refrigerant is drawn into cylinder through a suction valve during suction stroke of the piston, then the piston compresses the refrigerant and pushes it out through a discharge valve during discharge stroke. Suction and discharge valves are usually located in the cylinder head. The reciprocating compressor may be open, hermetic, or semi-hermetic type. A compressor whose crankshaft extends through the compressor housing so that a motor can be externally coupled to the shaft is called open-type compressor. A seal must be used where the shaft comes through the compressor housing to prevent refrigerant from leaking out. In hermetic-type compressor, motor and compressor are enclosed in the same housing to avoid the leakage at the seal. In this case, the motor is electrically insulated to operate even though it is in contact with refrigerant. The cold suction gas is drawn across the motor to keep the motor cool. Hermetic compressors are employed from 19th century and widely used in domestic refrigerators, air-conditioners because of their simplicity and flexibility of refrigeration capacity.

Many mathematical models and simulations of reciprocating compressors are available in open literature. Navarro et al. [1] proposed a new model for reciprocating compressors. The model solves out the general efficiency and volumetric efficiency by employing 10 empirical parameters that can be determined by curve fitting of experimental results. They proposed a curve fitting method based on Monte Carlo method that allows using some experimental results from the compressor's catalogue for curve fitting. Bin Yang et al. [2] proposed a comprehensive model for a semi-hermetic CO2 compressor. The model consists of three sub-models that simulate kinematics, compression process and friction losses. The model is validated for compressor

power and mass flow rate. Damle et al. [3] proposed an object oriented numerical simulation. Pe´rez-Segarra et al.[4] proposed a thermodynamics model calculating volumetric efficiency, isentropic efficiency and combined mechanical-electrical efficiency. Klein [5] proposed a semi-analytical model determining performance curve of a compressor. The model is validated by employing a calorimetric experimental setup. Refrigerant-12 is used as a heat source while cooling the condenser by a chiller. Flesch and Normey-Rico [6] designed a calorimeter for evaluating the performance of a refrigeration compressor; they proposed a model to calculate the performance parameters by using measured data.

In this study, designing, manufacturing and performance testing processes of a semi-hermetic, 4-piston refrigeration compressor is presented. All the processes are based on domestic facilities. The processes presented in this study are design, material selection, stress analysis, compressor manufacturing, motor design, manufacturing the rest of the compressor's components, and design and manufacturing of calorimetry.

MATERIAL AND METHODS

The Compressor

Thermodynamics design calculation of the compressor is done according to the model given by Bin Yang et al. [2]. Some geometrical dimension of the designed compressor is given in Table 1. The design of the compressor is done by using Solidwork (see Fig. 1). All of the components of the compressor are manufactured in Turkey.

Table 1. Compressor dimensions

Type	*Semi-hermetic reciprocating refrigeration compressor*
Number of piston	*4*
Bore diameter	*55 mm*
Stroke	*39,5 mm*
Revolution	*1450 rpm*
Displacement rate	*0.009072 m3/s*

Material selection

The microstructural investigation and chemical analysis of compressor bodies are performed in Bock and Bitzer compressors in order to enlighten material selection of the designed compressor in this work. The cross sections of both compressors are subjected to metallographic investigation. The sample surfaces are grounded using 120,240,320,600,800 and 1200 mesh papers and polished using 6, 3 and 1μm diamond solutions. Fig. 2 and 3 show microstructural images of Bock and Bitzer compressor bodies and engine crank surfaces, respectively. The microstructural investigation of piston materials is performed for both compressors. Fig.4 shows microstructural investigation results of both piston materials

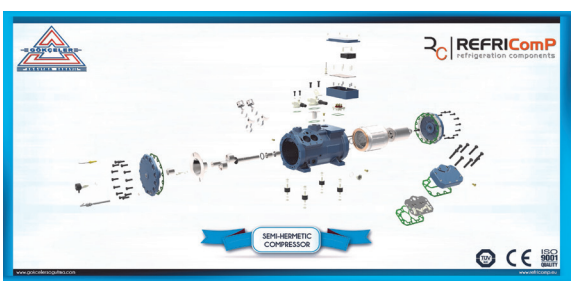

Figure 1. Explosion of designed and manufactured compressor

The systematic investigation is carried out for compressor body material selection as shown in Fig. 2 to 4. These systematic investigations lead to the selection of compressor body materials as GG 25. The chemical analysis results of the designed compressor body material are given in Table 2. Standard E-145 and E-171 are selected as piston and rod materials.

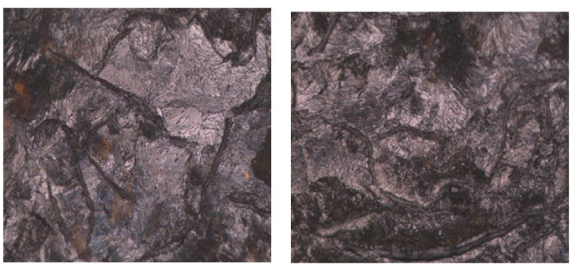

(a) (b)

Figure 2. Microstructures of compressor (a) Bitzer trademark (b) Bock trademark

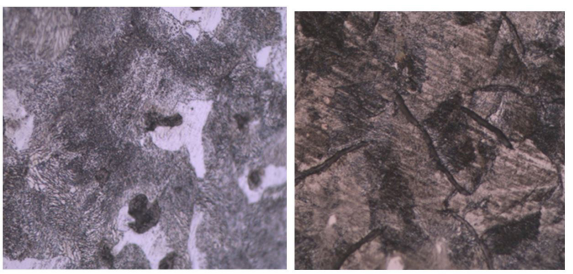

(a) (b)

Figure 3. Microstructure of compressor crank and connecting rod surfaces (a) Bitzer trademark (b) Bock trademark

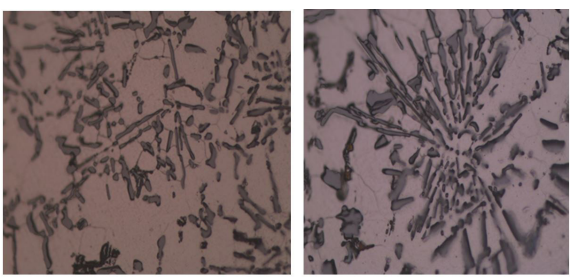

(a) (b)

Figure 4. Microstructures of piston materials (a) Bitzer trademark (b) Bock trademark

Table 2. The chemical composition of the designed compressor body material

Material	C	Si	Mn	P	Si
GG25	3.28	2.14	0.750	0.014	0.023

Structural Reliability of Critical Parts

Compressor body and crankshaft are evaluated to be the most critical parts to check structural reliability because they are subjected to variable loading as a result of reciprocating motions. Therefore, displacement, strain and stress distributions of compressor body and crankshaft are analyzed using Finite Element Method by means of Solidworks Professional (Dassault Systèmes SOLIDWORKS Corp., Waltham, Massachusetts, USA). The membrane valve controlling the flow of cooling gas is not analyzed specifically because it is more prone to failure due to fatigue. Structural analysis of compressor body is executed for the conditions representing explosion of pressure tanks. According to this, a 4.6 MPa pressure is applied all over the inside of compressor body without assembling crankshaft, pistons and electric motor with caps kept closed. If compressor body can bear this much loading conditions, it is safe for service conditions which are less critical. For instance, maximum pressure experienced in service is 2.3 MPa and it occurs only inside of cylinders, not all over the inner side of compressor body. The Von-Misses stress distribution and displacement distribution for the compressor body under 4.6 MPa pressure is given in Figure-5 below. As can be seen from Fig. 5, the maximum stress (198 MPa) occurs around the center of cap at the pistons side. Compressor body is made of cast iron (GG25) and the maximum stress is much lower than the ultimate tensile strength of GG25. Ultimate tensile strength is approximately 327 MPa based on tensile testing of material. Maximum displacement is around 0.1432 mm and it is evaluated to a small displacement which does not lead to yielding. Considering the fact that analysis conditions are tougher than the actual service conditions, it is concluded that compressor body is structurally reliable. For the crankshaft dynamic conditions are necessary to be considered in the analysis due to its high angular velocity. For this purpose, a quasi-static approach is utilized where the maximum possible inertial loads are applied statically to the shaft. Velocity and accelerations are calculated based on rotational velocity created by electric motor. Pressure loads coming from piston heads and inertial effects determines the loading conditions on the crankshaft transferred by connecting rods. For one round of a crankshaft, all the loads are determined and the most critical case is determined to be 5373 N, 3063 N, 1719 N and 2243 N coming from all four connecting rods in the angles of 0˚, 93˚, 180˚ and 246˚ respectively. Crankshaft is constrained on one bearing radially, axially and tangentially while it is constrained only radially on other bearing. With this type of boundary set up, the worsening effect of torque coming from electric motor is also taken into account for the most conservative estimate for reliability.

The maximum Von-Misses stress under these conditions is turned to be 184 MPa for the crankshaft and the maximum displacement is about 0.057 mm. These values are quite safe when the strength values of crankshaft material (forge steel) are considered. These analyses proved the structural reliability of compressor body and crankshaft under static and quasi-static conditions respectively. However, a modal analysis may also be necessary especially under high rate of rotational speeds. Modal analysis is also executed using Solidworks Professional and the frequencies for the first five modes are found to be 1680.7 Hz, 3585.5 Hz, 4996.2 Hz, 5304.6 Hz and 7749.9 Hz. The angular speed for service conditions is 24.16 Hz (1450 rpm) and this is much smaller than the frequency of first mode. Therefore, it is predicted that vibrations will not be a problem under the set-up considered in this compressor.

The Motor

In this study, three phase squirrel cage induction motor has been chosen as the drive motor of the compressor due to suitable for semi-hermetic refrigeration compressor and ease of manufacture. Design power of the compressor is 7.5 kW and revolutions per minute are 1450 rpm. In order to provide 7.5 kW output power of the motor, stator and rotor core length has been chosen as 120 mm.

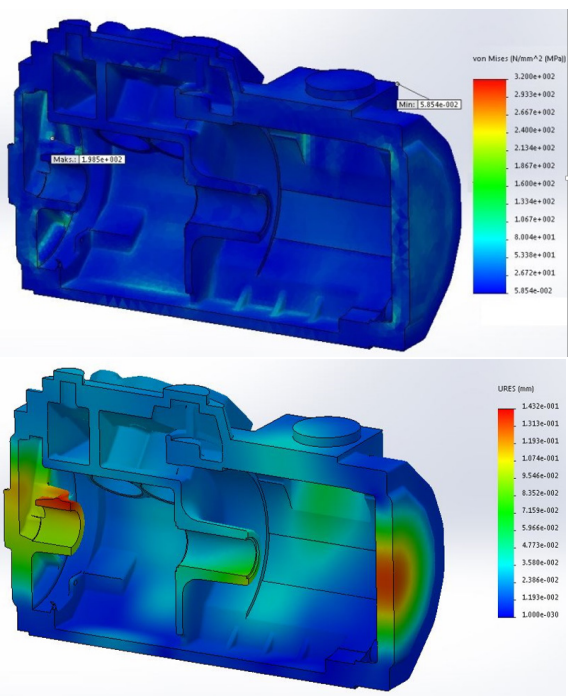

Figure 5. Finite element analysis results for compressor body (a) Von-Misses stress distribution (b) Displacement distribution

Table 3. Data for the designed induction motor

Number of stator slots	*36*
Outer diameter of stator	*190 mm*
Outer diameter of stator	*114 mm*
Number of conductor per slot	*27*
Number of wires per conductor	*3*
Wire diameter	*0.861 mm*
Slot filling factor	*51.2 (%)*
Number of rotor slots	*32*
Air gap	*0.5 mm*
Inner diameter of rotor	*32.65 mm*
Skew width	*1 slot*

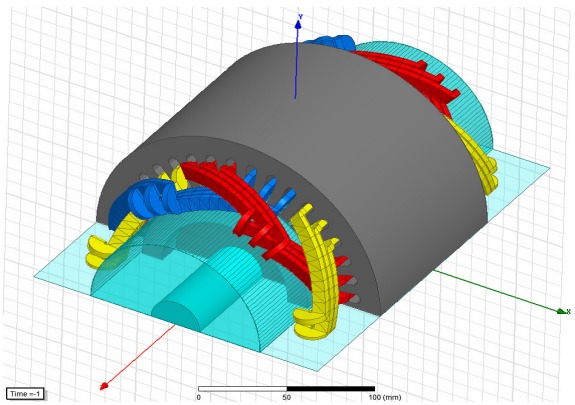

Figure 6. The cross-sectional image of the designed induction motor

In order to get desired speed, stator windings have been chosen as 4 poles. Since the compressor and motor will be in the same body, the stator outer and inner diameter values are defined as given in the Table 3. Performance analysis of the motor was carried out by using Maxwell, which software is using analytical and finite elements methods. As a result of the analysis, the motor is manufactured according to the data, which are given in Table-3 and placed in the main body of the compressor. Since the insulation of the winding wires is manufactured according to the coolant flow, the stator slot filling factor has been chosen about 50%. The cross-sectional image of the designed induction motor is given in Fig. 6.

Design and Manufacture of Calorimetric Setup

A calorimetric experimental setup is designed to determine the coefficient of performance (COP) of the manufactured compressor. The illustration of the setup is shown in Fig. 7. After charging oil into the manufactured compressor, it is connected to the setup. An oil separator is used after compressor exit to ensure a precise mass flow rate measurement of the working fluid, which is Refrigerant-404A.

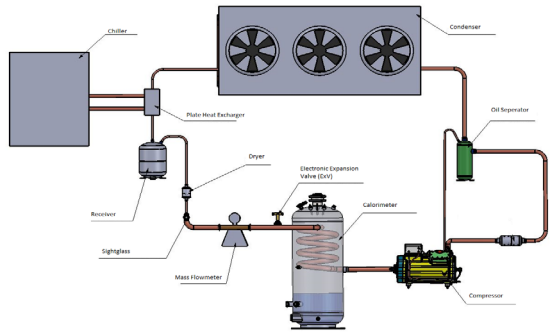

Figure 7. Calorimetric Experimental Setup

An air-cooled condenser with PID controlled-fan is used in the setup. The PID control on the condenser fan allows regulating the condensation temperature. The condenser unit is placed in outdoor environment. A plate heat exchanger (PHE) is used as subcooler that is connected to a chiller unit. Depending on the outdoor temperature, incomplete condensation may occur in the condenser. The subcooler ensures a complete condensation. Otherwise, incomplete condensation results in unstable working conditions, as a result, the system does not reach to steady conditions in case of incomplete condensation.

The Working Principle of Calorimeter

The calorimeter is the most important equipment of the experimental setup. Basically, the calorimeter is a tank containing a helical coil, refrigerant-134a, and electrical heater as it is seen from Fig. 8. R-404A, which is the working fluid of the experimental setup, boils while flowing through the coil. Heat sink to the coil is R-134a which is available at the bottom of the tank. The heater is immersed into liquid R-134a. The heater causes liquid R-134a to evaporate. And vapor of the R-134a rises and contacts to the coil and condenses on it while R-404A evaporates inside the coil. The state of R-404A is superheated vapor at the coil exit. The core idea designing the calorimeter is to provide an isothermal heat sink to the working fluid of R-404A. Charging pressure of the R-134a inside the tank is around 6 bar corresponding 20 °C saturation temperature. The heater is equipped with PID-capacity control that changes the heater power to ensure a desired super-

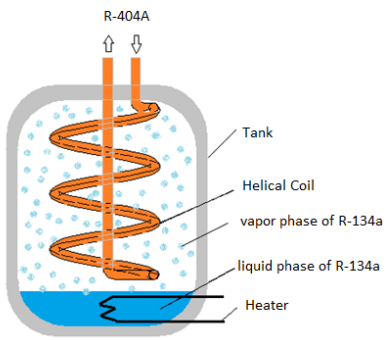

Figure 8. Calorimeter

heat of R-404A. Because refrigeration capacity of a compressor is given according to the superheat at the compressor inlet in compressor's catalogues, the superheat value is attained as a control parameter. The PID control of the heater measures the temperature of R-404A at the inlet of the coil and calculates desired temperature of the R-404A at the exit of the coil by adding a set value of superheat to the inlet temperature. The PID control arranges the heater power according to difference between the desired and the measured exit temperature.

The Calculations of Calorimeter

Heat transfer surface area of the coil and the pressure drop across the coil are important parameters for designing the coil. Heat transfer surface area of the coil is calculated as follow,

$$A_{s,coil} = \frac{Q_{ev}}{U \times \left(T_t - T_{ev}\right)} \tag{1}$$

where As,coil, Q_{ev}, U, T_t ,T_{ev} denote surface area of the coil based on outer diameter, refrigeration capacity of the compressor, overall heat transfer coefficient of the coil, saturation temperature of the fluid inside the tank (R-134a), and evaporation temperature of the fluid flowing inside the coil, i.e., R-404A, respectively. Qev in Eq. 1 must be the maximum refrigeration capacity of the compressor.
Total tube length of the coil,

$$L_{coil} = \frac{A_{s,coil}}{\pi \times d_o} \tag{2}$$

where Lcoil is the open length of the coil tube, and do is outer diameter of the tube. The inner diameter of the tube is determined by calculating pressure drop.

Overall heat transfer coefficient for the coil is calculated as follows,

$$U = \frac{1}{\frac{1}{h_{coil,i}} + \frac{1}{h_{coil,o}}} \tag{3}$$

where $h_{coil,i}$ and $h_{coil,o}$ stand for convective heat transfer coefficient inside and the outside of the coil, respectively. The thermal resistance of the tube wall is ignored in Eq. 3.

Convective heat transfer coefficient inside the coil, hcoil,i, is called convective boiling heat transfer coefficient (CBHTC) in the literature. Correlations are available for CBHTC in helical coil [7-11]. The most famous one among those correlations is Schrock–Grossman's correlation [7,8]. Zhao et al.[8] made some modifications on Schrock–Grossman's correlation to make it more accurate, namely the accuracy of the modified correlation is around %12. The modified Schrock–Grossman's correlation is given below,

$$\frac{h_{coil,i}}{h_{lo}} = 1.6\left(\frac{1}{X_{tt}}\right)^{0.74} + 183{,}000B_o^{1.46} \tag{4}$$

$$h_{lo} = \frac{1}{41} Re_{lo}^{5/6} Pr_l^{0.4} \left(\frac{d_i}{D_{helix}}\right)^{1/12} x\left(1 + \frac{0.061}{\left(Re_{lo}\left(d_i / D_{helix}\right)^{2.5}\right)^{1/6}}\right)\frac{k_l}{d_i} \tag{5}$$

$$Re_{lo} = \frac{Gd_i}{\mu_l} \tag{6}$$

$$X_{tt} = \left(\frac{1-x}{x}\right)^{0.9}\left(\frac{\rho_g}{\rho_l}\right)^{0.5}\left(\frac{\mu_l}{\mu_g}\right)^{0.1} \tag{7}$$

$$B_o = q / G * i_{fg} \tag{8}$$

$$G = \frac{\dot{m}_r}{A_c} \tag{9}$$

$$q = \frac{Q_{ev}}{A_{s,coil}} \tag{10}$$

where $h_{coil,i}$ is CBHTC, h_{lo} and Re_{lo} are liquid only heat transfer coefficient and Reynolds number for the total flow assumed to be liquid, d_i inner diameter of coil tube, D_{helix} is helix diameter of coil, X_{tt} is Martinelli parameter, B_o is boiling number, i_{fg} is enthalpy of vaporization, $\dot{m}_r$ is mass flow rate of working fluid, G is mass flux, q is heat flux, Q_{ev} evaporation heat rate in the coil or another saying compressor refrigeration capacity, As,coil is coil surface area, A_c is cross-sectional area of coil tube, and the subscript lo denotes for liquid only.

CBHTC, $h_{coil,i}$, in Eq. 4 is calculated depending on the quality, namely, x. Therefore, the local hcoil,i is calculated by incrementing the quality, dx, from its value at the inlet of the coil to unity. Then, integral average of $\bar{h}_{coil,i}$ is calculated as follows,

$$\bar{h}_{coil,i} = \frac{\int_{x_i}^{1} h_{coil,i}\, dx}{1 - x_i} \tag{11}$$

The quality at the coil inlet is calculated by using the correlation given below,

$$x_i = 0.00675\left(1 + 0.00167T_{cd,e} + 0.00472T_{ev}\right)\left(T_{cd,e} - T_{ev}\right) \tag{12}$$

where $T_{cd,e}$ is temperature of working fluid (R-404A) at coil exit, Tev is evaporation temperature inside the coil. Because laminar film condensation occurs at outer surface of the coil, i.e., tank side, the correlation known as Nusselt theory [12] is used for the tank side heat transfer coefficient.

$$h_{coil,o} = 0.729\left[\frac{g\rho_l(\rho_l-\rho_v)k_l^3 i_{fg}^{'}}{\mu_l(T_{cd}-T_w)d_o}\right] \quad (13)$$

where subscript v stands for vapor phase, T_{cd} is condensation temperature of R-134a inside the tank, T_w is wall temperature of the coil that is calculated as follows,

$$T_w = \frac{q}{h_{coil,i}} + T_{ev} \quad (14)$$

The parameter i_fg^' in Eq. 3 is calculated as follows,

$$i_{fg}^{'} = i_{fg} + 0.68c_{p,l}(T_{cd}-T_w) \quad (15)$$

The coil surface area is calculated according to the flowchart given in Fig 9.

When the pressure drop is calculated, it must be taken into consideration that the flow is two-phase and the construction of the coil is helix. Two-phase flow pressure drop in a helical coil is calculated by using the correlation given by Zhao et.al.[8]. The correlation is given briefly for the reader convenience. Generally, the two-phase frictional multiplier is employed to correlate the frictional pressure drop of two-phase flow. Its definition is

$$\varnothing_{lo}^2 = \frac{\Delta P_{TP}}{\Delta P_{lo}} \quad (16)$$

where ΔP_{TP} is the two-phase flow frictional pressure drop and ΔP_{lo} is the single-phase frictional pressure drop. Zhao et al. [8] suggested following correlation, which has an uncertainty of ±15%, for the two-phase frictional multiplier.

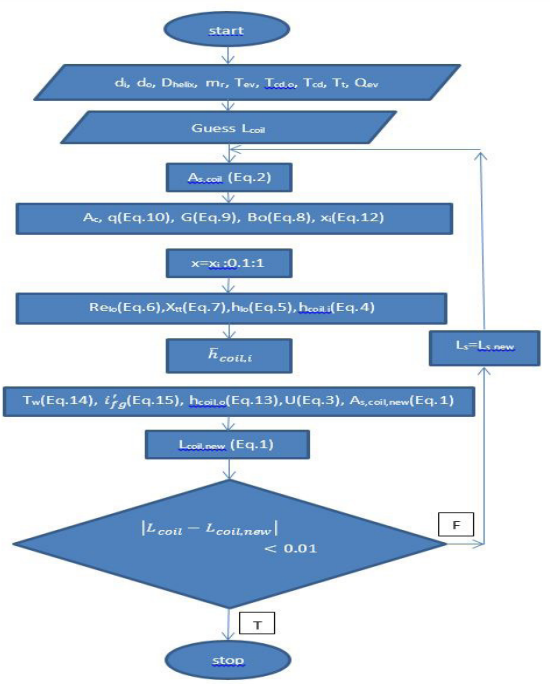

Figure 9. Flowchart

$$\varnothing_{lo}^2 = 1 + \left(\frac{\rho_l}{\rho_g}\right)\left[0.303x^{1.63}(1-x)^{0.885}Re_{lo}^{0.282} + x^2\right] \quad (17)$$

Friction factor for single-phase flow in helical coil is calculated by using White correlation [8].

$$f = 0.08Re_{lo}^{-1/4} + 0.012(d_i / D_{helix})^{1/2} \quad (18)$$

The single-phase frictional pressure drop is calculated as follows,

$$\Delta P_{lo} = 4f\frac{L_{coil}}{d_i}\frac{G^2}{2\rho} \quad (19)$$

where Lcoil is total tube length of the coil and G is the mass flux.

Because the pressure drop through the coil is fulfilled by the tested compressor, the higher the pressure drops inside the coil, the lower the COP of compressor. Therefore, the two-phase flow frictional pressure drop calculated according to Eqs. 16-19 must be minimal for designing helical coil.

Refrigeration Capacity Calculations of the Compressor

The mass flow rate of the working fluid is measured by a mass flowmeter. Thermodynamic properties of the working fluid (R-404A) are calculated by using the equations given by Sözen et.al. [13].

Refrigeration capacity of the compressor is calculated as follows,

$$\text{SPT} = \frac{P_{fc}.C_{fc}}{\left[\quad\quad\right]} \quad (21)$$

where $\dot{m}_r$, $i_{coil,e}$ and $i_{coil,i}$ are mass flow rate and the enthalpies of the working fluid at inlet and outlet of the compressor.

The volumetric efficiency of the compressor is calculated as follows,

$$\eta_v = \frac{\dot{m}_r}{V_{sw}} \times v_{com,i} \quad (22)$$

where $v_{com,i}$ is specific volume of the working fluid at the compressor inlet.

The isentropic efficiency of the compressor is calculated as follows,

$$\eta_i = \dot{m}_r \frac{i_{com,isen} - i_{com,i}}{P_m} \quad (23)$$

where $i_{com,isen}$ is the isentropic enthalpy of working fluid at the compressor exit, $i_{com,i}$ is the enthalpy of the working fluid at the compressor inlet, P_m is the electrical power of the

motor. V_{sw} is the displacement rate of the compressor and it is calculated as follows,

$$SPT_{chp} = \frac{C_{fc} \cdot P_{fc}}{AEP\left[C_{el} - \frac{C_{fuel}}{\eta_{el}} + \left(\frac{\eta_{hst}}{\eta_{el}} - 1\right) f_{hst} \cdot \frac{C_{fuel}}{\eta_{heat}}\right]} \quad (24)$$

where N_{cy} is number of cylinder (4), D_{cy} is diameter of cylinder (55mm), H is stroke (39.5mm), n is revolution per minute (1450 rpm).

Refrigeration coefficient of performance of the compressor (COPR) is calculated as follows,

$$COP_R = \frac{\dot{Q}_{ev}}{P_m} \quad (25)$$

Where $\dot{Q}_{ev}$ is calculated by using Eq. 21.

Condenser heat capacity is calculated as follows,

$$\dot{Q}_{cd} = \dot{m}_r \left(i_{cd,e} - i_{cd,i}\right) \quad (26)$$

Where $i_{cd,e}$ and $i_{cd,i}$ are enthalpy of working fluid at outlet and inlet of the condenser.

Subcooler heat rate is calculated as follows,

$$Q_{sc} = \dot{m}_r \left(i_{sc,e} - i_{sc,i}\right) \quad (27)$$

where $i_{sc,e}$ and $i_{sc,i}$ are the enthalpies of working fluid at exit and inlet of subcooler.

Motor work rate is calculated as follows,

$$\dot{W}_{com} = \dot{m}_r \left(i_{com,e} - i_{com,i}\right) \quad (28)$$

Overall efficiency of the compressor is calculated as follows,

$$\eta_{com,g} = \frac{\dot{W}_{com}}{P_m} \quad (29)$$

where $\dot{W}_{com}$ is calculated by using Eq. 28, P_m is the motor power that is measured.

MEASUREMENT, DATA ACQUISITION AND CONTROL

Working principle and control of the experimental setup

The automation, control and data acquisition system of calorimetric experimental setup work on following principle: simultaneous data reading from the sensors on the setup, saving those data on PLC, converting the saved data to desired units, inserting the converted data to the mathematical model given n the previous section and saving results, activating or inactivating required control functions depending on those saved results, rearranging analog outputs of some of the control functions and then saving the yielded raw data, converted data and results of calculations on arrays of PLC, importing those data arrays to a USB file through USB port located on HMI.

Instrumentation

Uninsulated, flat-surface PT100 and PT1000 sensors are used for temperature measurements to ensure a short response time and high accuracy. Also, these sensors are placed into their slots on the experimental setup by applying heat transfer paste. The uncertainty and conversion accuracy of the PT100 and PT1000 sensors are ± 0.1 °C, ± 0.01 °C and 0.1 °C, 0.01 °C, respectively. Analog signals of the sensors are transferred to the PLC via PT100/PT1000 data input module of the PLC's manufacturer.

Pressure transmitters are chosen as 4-20mA output signal, because of possible static electricity and EMI effects. Analog signals of the transmitters are transferred to the PLC via 4-20mA data input module of the PLC's manufacturer. Measuring range of the transmitters is chosen in two different types due to pressure level of the system. Meanwhile, -0.8 to 7 bar measurement range is chosen in low level pressure part of the system, 0 to 30 bar measurement range is chosen in high level pressure part of the system.

Energy analyzer is used to measure electrical current, voltage, cosØ, frequency, and both real time and total consumption of power. In measurement of the current, the current transformators are used, which have C1:0.5 accuracy class and they are certified by UEDAŞ laboratory. Data acquisition between energy analyzer and PLC is done via RS 485/2 port by using MODBUS RTU protocol with 38,600 bps.

Rotational speed of the condenser fans and subcooler pump are controlled with an AC inventer and the power of the heaters is controlled by a SRC unit with 50 kW. Both the inverter and the SRC are controlled by the PLC. Mass flow rate of the working fluid of R-404A is controlled by using electronic expansion valve (ExV) that has a DANFOSS® EKD 316 superheat controller. Data acquisition between the superheat controller and PLC is done via RS 485/2 port by using MODBUS RTU protocol with 38,600 bps.

A Coriolis type mass flowmeter is used for measuring mass flow rate of R-404A. Data acquisition between the flowmeter and PLC is done via RS 485/2 port by using MODBUS RTU protocol with 38,600 bps. The oil flow rate is measured by using a mass flowmeter with pulse signal output that is converted to desired units via high speed HSC counter placed on the PLC.

A touch-screen with high resolution HMI is used to start the experimental setup, enter the input parameters, and monitor tables, graphics and analogue or digital data. The HMI has a large data saving capacity and it is capable

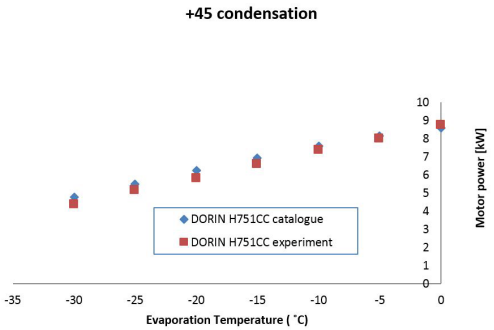

Figure 10. Experimental validation of the calorimetric setup: the motor power consumption.

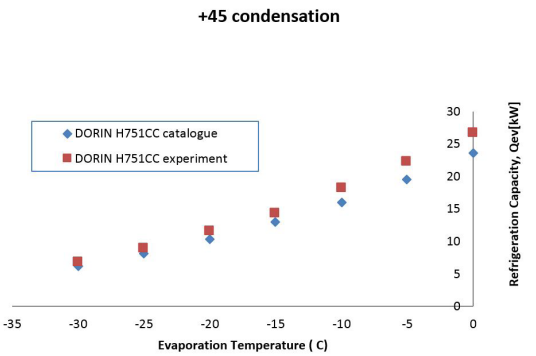

Figure 11. Experimental validation of the calorimetric setup: Refrigeration Capacity

to import data to USB. Data acquisition between HMI and the PLC is done via RS 232 port by using MODBUS RTU protocol with 115,200 bps.

A high speed PLC having a particular MCU that is capable of doing 32 bite float mathematical operations is preferred. The PLC has a CPU with 19 ns cycle speed. Analog to digital conversion of all analogue sensors and transmitters is done in 69 ms and also finishes all of the communications via MODBUS RTU protocol in 160 ms. The cycle duration for the entire programme 97 ms and the programme runs independent of communication process.

Besides the equipment mentioned above, various relays, fuses, power contactors, and terminal blocks are used.

RESULTS AND DISCUSSION

The coil, i.e., evaporator, is designed by a code written according to the flowchart based on the model given n the previous sections. Considering manufacturing limitations, inner diameter of coil tube and helix diameter of the coil are attained as d_i = 12 mm and D_{helix} = 125 mm, respectively. As results, the total tube length of the coil is calculated 43 m and corresponding pressure drop is calculated as 18.7 MPa, which is unacceptable. Governing parameters on the pressure drop are tube diameter, total tube length and mass flow rate. It is not reasonable to increase the tube diameter because of manufacturing limitations. The largest tube diameter that we enable to manufacture coil is limited to ½ inch. Therefore, in order to decrease the pressure drop, the total length of the tube is divided into 7 parts and 7 identical helical coils are manufactured. The flow rate for every coil is decreased by one out of seven in this case. Therefore, decreasing the tube length and flow rate one out of seven, it is expected to decrease the pressure drop dramatically because the tube length and the flow rate for any coil are a multiplier factors as it is seen from Eqs. 16 to 19. Thus, running the code again with this new design approach yields 0.054 MPa of pressure drop that is acceptable. As a result, 7 identical helical coils are manufactured, one of the helical coils is placed on center and while the rest are placed in circumference of the tank. A refrigerant distributor is used to ensure an equal mass flow through each coil.

As it is mentioned before, R-134a as a seconder fluid is charged into tank with 5.7 bar and 20 °C. A sight glass is placed on the tank wall at the bottom side for surveillance if the liquid level of the R-134a above the heaters. Besides, pressure and temperature inside the tank are measured with a pressure transmitter and a PT100 sensor to check if the design conditions are satisfied.

Because the calorimetric experimental setup is our own product, first of all, experimental validation is necessary. For this purpose, a H751CC model DORIN® compressor that is European original trademark is tested via the calorimetric experimental setup and the measured performance parameters are compared with those given in the compressor's catalog. Results are given in Fig. 10 to 12.

Fig. 10 shows the comparison of the motor power while Fig. 11 is showing refrigeration capacity. As it is seen from those figures, values given in the catalog for both motor power and refrigeration capacity are in good agreement with those experimentally measured data by using the setup. Refrigeration COP of the compressor is compared in Fig. 12. As it is seen from the figure, the deficiency between the measured values and catalog values for COPR are around 11-15 % . The uncertainty calculated by using the method given by Kline and McClintock [14] for the COPR is±10.3%. Considering the uncertainity of ±10.3% and the uncertainity of the catalog's values, the deficiency in Fig. 3 is in acceptable limitations. As results Fig. 10 to 12 shows that the validity of

Table 4. Design results of the coil

L_{coil}	$A_{s,coil}$	item	d_o	d_i	D_{helix}	ΔP_{TP}	m_r	U	T_{cd}	T_{ev}	Q_{ev}
m	m2		mm	mm	mm	bar	kg/s	W/m²K	˚C	˚C	W
6.77	0.27	7	12.7	12	125	0.54	0.0434	1338.99	30	5	5428

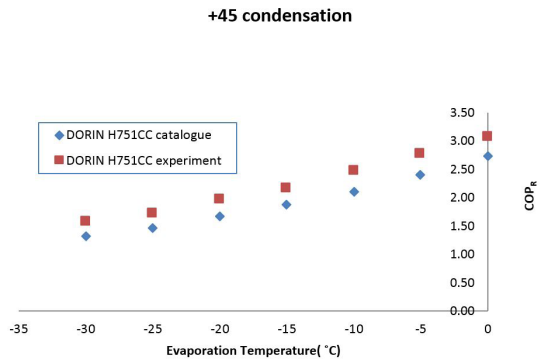

Figure 12. Experimental validation of the calorimetric setup: Refrigeration coefficient of performance

test results from the experimental setup is always reliable.

After validating the experimental setup, the manufactured compressor is tested by employing the setup. The parameters such as refrigeration capacity, motor power and COPR, which are necessary performance parameters that

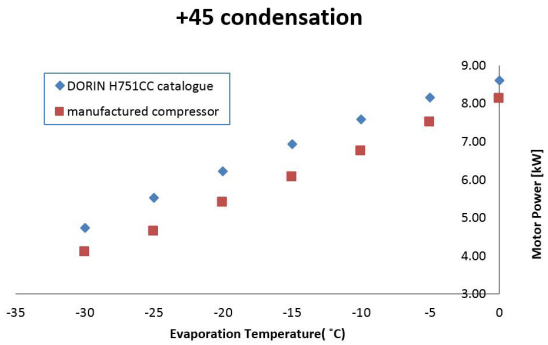

Figure 13. The motor power consumption

a compressor catalog must contain, are determined and a compressor catalog is prepared [15]. The performance parameters mentioned above are calculated by using the mean values of 50 measured data saving 30 s time intervals.

Fig. 13 shows the comparison of the motor power of the manufactured compressor and DORIN compressor.As seen, the manufactured compressor consumes less power comparing to DORIN. It is better to compare both of the

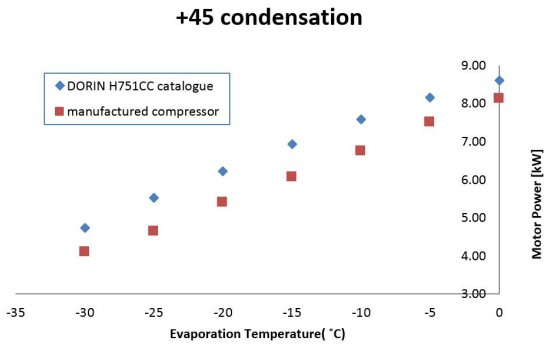

Figure 14. Refrigeration Coefficient of Performance

compressors with a dimensionless parameter of COPR. Fig. 14 shows the comparison of COPR of the compressors. As seen, the COPR of the manufactured compressor is higher than that of DORIN compressor's by around 12%. As a result, performance of the first domestic compressor of Turkey is as good as an equivalent European original.

ACKNOWLEDGEMENT

This project is implemented in corporation with Gökçeler Refrigeration Company, and funded by The Scientific and Technological Research Council of Turkey (TUBITAK) with the project number of TEYDEP1507- 7140320. The authors thank to TUBITAK and Gökçeler Refrigeration Company for their contributions.

Symbols and Abbreviations

Symbols		*Subscripts*	
q	*Heat flux [W/m2]*	*a*	*atmosphere*
Bo	*Boiling number*	*c*	*cross-sectional*
x	*Quality*	*cd*	*condenser*
H	*Stroke [m]*	*com*	*compressor*
Q	*Heat rate [W]*	*cy*	*cylinder*
i	*Enthalpy [kJ/kg]*	*e*	*exit*
T	*Temperature [˚C]*	*ev*	*evaporator*
$\dot{m}$	*Mass flow rate [kg/s]*	*i*	*inner, inlet*
d, D	*Diameter [m]*	*l*	*liquid*
L	*Length [m]*	*lo*	*liquid only*
k	*Heat conduction coefficient [W/mK]*	*m*	*motor*
G	*Mass flux [kg/m2s]*	*o*	*outer*
h	*Convective heat transfer coefficient [W/m2K]*	*r,R*	*refrigerant, refrigeration*
f	*Friction factor*	*s*	*surface*
A	*Area [m2]*	*sc*	*subcooler*
V	*Displacement [m3/s]*	*t*	*tank*
U	*Overall heat transfer coefficient [W/m2K]*	*TP*	*two-phase*
X_{tt}	*Martinelli number*	*v*	*volumetric*
n	*Rotational speed [rpm]*	*w*	*wall*
Abbreviations			
COP	*Coefficient of performance*	*PLC*	*Programmable logic controller*
PID	*Proportional–Integral–Derivative controller*	*HMI*	*Human Machine Interaction*
USB	*Universal Serial Bus*	*HSC*	*High speed counter*
PT	*Platinum temperature sensor*	*CPU*	*Central Process Unit*
ExV	*Electronic Expansion Valve*	*UEDAŞ*	*Uludağ Electric Company*
MODBUS RTU	*MODBUS Remote Terminal Unit*		

REFERENCES

1. Navarro E, Granryd E, Urchueguı JF, Corberan JM. A phenomenological model for analyzing reciprocating compressors. International Journal of Refrigeration 30(2007)1254 – 1265.
2. Yang B, Bradshaw CR, Groll EA. Modeling of a semi–hermetic CO2 reciprocating compressor including lubrication submodels for piston rings and bearings. International journal of refrigeration 36(2013) 1925 – 1937.
3. Damle R, Rigola J, Pe´rez–Segarra CD, Castro J, Oliva A. Object–oriented simulation of reciprocating compressors: Numerical verification and experimental comparison. International journal of refrigeration 34(2011)1989 – 1998.
4. Pe´rez–Segarra CD, Rigola J, So`ria M, Oliva A. Detailed thermodynamic characterization of hermetic reciprocating compressors. International Journal of Refrigeration 28(2005)57 – 59.
5. Klein SA. Develop Data Base for Determining Optimum Compressor Rating Points for Residential Refrigerator and Freezer Compressors. ASHRAE RP–870 (1999)
6. Flesch RCC, Normey–Rico JE. Modelling identification and control of a calorimeter used for performance evaluation of refrigerant compressors. Control Engineering Practice 18(2010)254 –261.
7. Elsayed AM, Raya K, Dadah AL, Mahmoud S, Rezk A. Investigation of flow boiling heat transfer inside small diameter helically coiled tubes. International Journal of Refrigeration 35(2002) 2179 – 2187.
8. Zhao L, Guo L, Bai B, HouY, Zhang X. Convective boiling heat transfer and two–phase flow characteristics inside a small horizontal helically coiled tubing once–through steam generator. International Journal of Heat and Mass Transfer 46(2003) 4779 – 4788.
9. Chung YJ, Bae KH, Kim KK, Lee WJ. Boiling heat transfer and dryout in helically coiled tubes under different pressure conditions. Annals of Nuclear Energy 71(2014) 298 – 303.
10. Wongwises S, Polsongkram M. Evaporation heat transfer and pressure drop of HFC–134a in a helically coiled concentric tube–in–tube heat exchanger. International Journal of Heat and Mass Transfer 49(2006) 658 – 670.
11. Cui W, Li L, Xin M, Jen TC, Chen Q, Liao Q. A heat transfer correlation of flow boiling in micro–finned helically coiled tube. International Journal of Heat and Mass Transfer 49(2006) 2851 – 2858.
12. Kakaç S, Liu H. Heat Exchangers: Selection, rating and thermal design. CRC Press, 2012.
13. Sözen A, Arcaklioğlu E, Menlík T. Derivation of empirical equations for thermodynamic properties of a ozone safe refrigerant (R404a) using artificial neural network. Expert Systems with Applications 37(2010)1158 – 1168.
14. Holman JP. Experimental Methods for Engineers, 6th ed., McGraw–Hill, Singapore, 1994.
15. Gökçeler A.Ş., http://www.gokcelersogutma.com.tr/